

# PARAMETER ESTIMATION AND DATA-DRIVEN METHOD FOR FOREST FIRE PREDICTION

X. LI<sup>1,2\*</sup>, C. TANG<sup>1</sup>, M. ZHANG<sup>1</sup>, S. ZHANG<sup>1</sup>, S. LI<sup>1,2</sup>, Y. WANG<sup>1,2</sup>, S. SUN<sup>3</sup>, J. LIU<sup>1,2</sup>

<sup>1</sup> College of Mechanical and Electrical Engineering, Northeast Forestry University, Harbin 150040, China;

<sup>2</sup> Forestry Artificial Intelligence and Equipment Engineering Technology Research Center of the State Forestry and Grassland Bureau, Northeast Forestry University, Harbin 150040, China;

<sup>3</sup> College of Engineering and Technology, Northeast Forestry University, Harbin 150040, China

\*Corresponding Author

---

**ABSTRACT.** Improvement in the accuracy of the forest fire prediction model is essential to properly instruct firefighting forces. The input parameters of traditional prediction method cannot be adjusted in real-time, so the forecasting accuracy will decrease over time. To solve this problem, the forest fire prediction system based on parameter estimation and data-driven method is proposed in this paper. First, two dynamic parameters based on the empirical formula, rate of fire spread and main spreading direction, and multi-sensor data are input to a forward prediction model based on the Huygens principle to generate the predicted fireline for the current time. Secondly, the difference between the predicted and observed firelines is minimized by the Grey Wolf Optimization algorithm, which derives the optimal dynamic parameters. Finally, the optimal parameters and the current multi-sensor data are input into the prediction model to achieve accurate prediction of the fireline. The burn experiment was designed, and the feasibility of the system was verified by real fire data. The results indicate that a fire prediction system that quickly calibrates dynamic input parameters is developed and can achieve real-time accurate fire predictions.

**Keywords:** parameter estimation; Grey wolf optimization; data-driven; fireline prediction

---

## 1 BACKGROUND

Forest fires are characterized by high suddenness, destructive power and difficulty in extinguishing, and can cause serious damage to economy and ecology (Cardil et al., 2021). In the event of a fire, computer simulation techniques for fire behavior trend prediction can be applied to rationalize fire suppression strategies and thus reduce damage (Monedero et al., 2019). Many fire spread models have been proposed, such as McArthur model, Rothermel model, and Wang Zhengfei model (Griffiths, 1999; Rothermel, 1972; Wang, 1983). On this basis, Farsite, Phoenix, Prometheus (Finney, 1998; Tolhurst et al., 2008; Tymstra et al., 2010) and other fire simulators have been produced. But all these fire spread models are simplified empirical models, and under the influence of complex environmental factors, the calculated and the real rate of fire spread (ROS) may differ significantly (Srivas et al., 2017). In addition, the coupling of the fire and wind may cause the synthetic main spread direction to differ from the true value (Anderson

et al., 2007). Prediction results can be affected by errors in ROS and main spread direction, so it is an important research aspect to correct them in time (Carrasco et al., 2019).

This problem can be effectively solved by the parameter estimation method (Altintas et al., 2015). The observed and predicted data are used for data assimilation to derive optimal parameters, which are input into the simulator together with the sensor data to improve prediction accuracy (Ferragut et al., 2015). In recent years, this idea has been applied by scholars to improve the accuracy of forest fire prediction. Mandel applied this idea to forest fire prediction by correcting the temperature and location state of the flames through EnKF and atmospheric coupled wildfire prediction model (Mandel et al., 2009), but it created problems of false predictions and excessive computational cost. Denham built a dynamic data-driven forest fire prediction application based on GA algorithm for wind value estimation (Denham et al., 2012), but a huge computational burden can be generated. Rochoux proposed

a kalman filter-based method for dynamic prediction of forest fire spread, which used observed fireline locations for ROS calibration (Rochoux et al., 2013). Alessandri adopted the level set approach to construct a model of the spatio-temporal standing evolution of forest fire, the differences between observed and predicted firelines were minimized by least-squares to achieve parameter estimates of topography and vegetation (Alessandri et al., 2021). However, the problems of high computational cost, poor real-time performance and weak adaptability of the algorithm to nonlinear forest fire systems are present in the above-mentioned papers.

To solve the above problems, a forest fire spread prediction system based on parameter estimation and data-driven method was proposed in this paper. First of all, a forward fire prediction model based on the Huygens principle was established. Initial dynamic variables, ROS and main direction, and multi-sensor data were input to the model to obtain the predicted fireline for the current time. Then the Grey Wolf Optimization algorithm was used to minimize the gap between the observed and predicted firelines and correct the dynamic variables. Then the optimal parameters and current sensor data were jointly input into the forward model for a real-time accurate prediction of fireline, thereby a forest fire prediction system based on parameter estimation and data-driven was established.

The paper is structured as follows: In Section 2, the experimental configuration and IR image processing process are presented. In Section 3, the structure of the parameter estimation and data-driven forest fire prediction system is introduced, mainly including the establishment of the forward spreading model, the design of the cost function, and the optimization method. The results and analysis of validating this system using real fire data are presented in Section 4. And the summary and the discussion of future work are presented in the conclusion (Section 5).

## 2 EXPERIMENT AND DATA PROCESSING

### 2.1 The Experimental Configuration and Data Acquisition

The burn experiment in this paper was carried out on October 29, 2021, in Pingfang District, Harbin City, Heilongjiang Province, where the combustible material was collected from the Maor Mountain of Heilongjiang Province, and the fuel type was the *Pinus sylvestris* needle. As shown in Fig. 1, the combustibles were all laid manually and can be identified as uniform, with a thickness of  $50.0mm$ ; the size of the combustible laying was  $5 \times 11.05m^2$  (there was a flat slope area of  $5 \times 3m^2$ ); by weighing the total mass of randomly sampled combustibles before and after drying, the moisture content

of fuel was calculated as 13.3%; the slope was  $8.305^\circ$ . The weather conditions: the average temperature during the experiment was  $15^\circ C$ , the relative air humidity was 28.0%, and the average and maximum wind speeds were  $6.8km/h$  and  $11.16km/h$ .



Figure 1: Burning experiment configuration. Shown from left to right are a set of wind sensor (only one of all sensors is framed), a marker point (only one of all markers is framed) and the M600Pro UAV with the infrared camera.

The experimental site was equipped with 4 sets of integrated wind speed and direction sensor, a DJI Matrice M600Pro UAV with a Flir Duo<sup>TM</sup> Pro R high-resolution thermal camera, and a visible light camera, which were respectively used to obtain real-time wind field data and infrared image data. The wavelength range of thermal imaging cameras is  $7.5 - 13\mu m$ , which can store infrared images with a resolution of pixels at a frequency  $9Hz$  quickly. 6 high-temperature objects were placed around the experimental site as marker points for subsequent geographic calibration of the IR images, enclosing a total area of  $6.05 \times 15m^2$ .

### 2.2 Fireline Extraction

The angle between the camera and the burn area causes the IR image to be spatially different from the actual scene, so image correction must be performed to obtain their orthogonal view (Yu et al., 2021). The original IR image can be transformed into its orthographic image after perspective transformation (Choi et al., 2006), and

the geographical information of the fireline is corrected. The perspective transformation formula is shown in the Eq. (1), where  $(u, v, w)$  and  $(x', y', z')$  are the pixel coordinates before and after the transformation, and  $a_{ij}$  is the  $3 \times 3$  perspective transformation matrix calculated by four marker points.

$$\begin{bmatrix} x' & y' & z' \end{bmatrix} = \begin{bmatrix} u & v & w \end{bmatrix} \begin{bmatrix} a_{11} & a_{12} & a_{13} \\ a_{21} & a_{22} & a_{23} \\ a_{31} & a_{32} & a_{33} \end{bmatrix} \quad (1)$$

As shown in Fig. 2(a), the green line is flat and sloped on both sides, so the conversion must be done separately and then spliced. Then, the converted image is smoothed by the median filtering method (Erkan et al., 2018), as shown in Fig. 2(b). Finally, the threshold segmentation (Norouzi et al., 2014) method is used to extract the fire boundary Fig. 2(c).

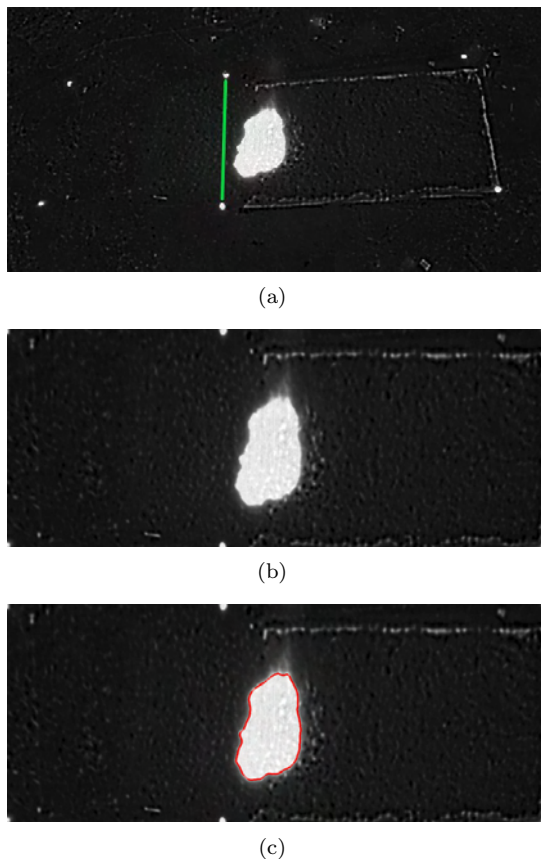


Figure 2: The process of extracting fireline from IR images. (a) Raw IR image. The green line was added to distinguish the flatland on the left from the slope on the right. (b) Image after perspective transformation and smoothing. (c) The red curve is the extracted fireline.

### 2.3 The Sorting of Discrete Points

The set of pixel points on the fire boundary extracted by image traversal is discontinuous and dense in the actual coordinate space, which is not conducive to computation. Thus, two discrete points sorting methods were proposed in this paper:

(1) The rays are drawn continuously from the fire center  $(x_c, y_c)$  at the angle of  $\lambda (\lambda \in (0, 2\pi))$ , the intersections with the fireline will be detected, and interpolation is performed when the distance between two adjacent points is higher than the threshold of  $0.25m$ . The result is shown in Fig. 3(a).

(2) The ordering is achieved according to the slope of the discrete points concerning the centroid  $(x_c, y_c)$ , and the points are taken at intervals of 5 to reduce the density of the discrete points. The result is shown in Fig. 3(b). The second way is simple and faster through testing, so it was chosen for discrete points sorting.

Eq. (2) captures the location of the center of the fire:

$$\text{Dis}(x, y) = \min \left( \sum_{i=1}^n (x_i - x)^2 + (y_i - y)^2 \right) \quad (2)$$

$\{(x_1, y_2) \cdots (x_n, y_n)\}$  is the set of all points on the fireline. The Nelder-Mead algorithm (Lagarias et al., 1998) is used to find the center  $(x_c, y_c)$  by minimizing the distance  $Dis$ .

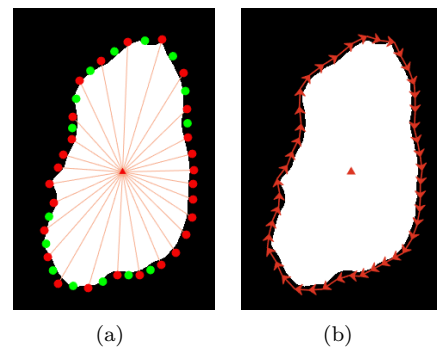


Figure 3: Schematic diagram of the discrete points sorting, and the triangle sign is the center of the fire. (a) Method 1 of the discrete point sorting. The red points are the intersections of the ray and the fireline, and the green points are the interpolation points. (b) Method 2 of the discrete point sorting. The vertices of the arrows are the extracted discrete fire points, which are ordered by the slope of the lines connected to the center point.

### 3 THE FOREST FIRE PREDICTION SYSTEM BASED ON PARAMETER ESTIMATION AND DATA-DRIVEN

#### 3.1 System Framework

The structure of the parameter estimation and data-driven forest fire prediction system (hereinafter collectively referred to as FFPS) is shown in Fig. 4, which is divided into the parameter estimation phase and the forecast phase. In the parameter estimation phase, the dynamic variables  $\delta(R, \theta)$  that based on empirical values, the wind speed  $\bar{v}_{T_i}$  and the true fireline  $\bar{L}_{T_i}$  are input to the forward prediction model to obtain the predicted fireline  $\hat{L}_{T_{i+1}}$ . The cost function  $J$  constructed from the observed and predicted firelines at a time  $T_{i+1}$  is minimized by the GWO algorithm to find a correct set of dynamic variable values  $\delta'(R, \theta)$ . In the prediction stage, the corrected dynamic variables  $\delta'(R, \theta)$  and the current sensor data are input into the forward model to obtain the predicted fireline  $\hat{L}_{T_{i+2}}$ .

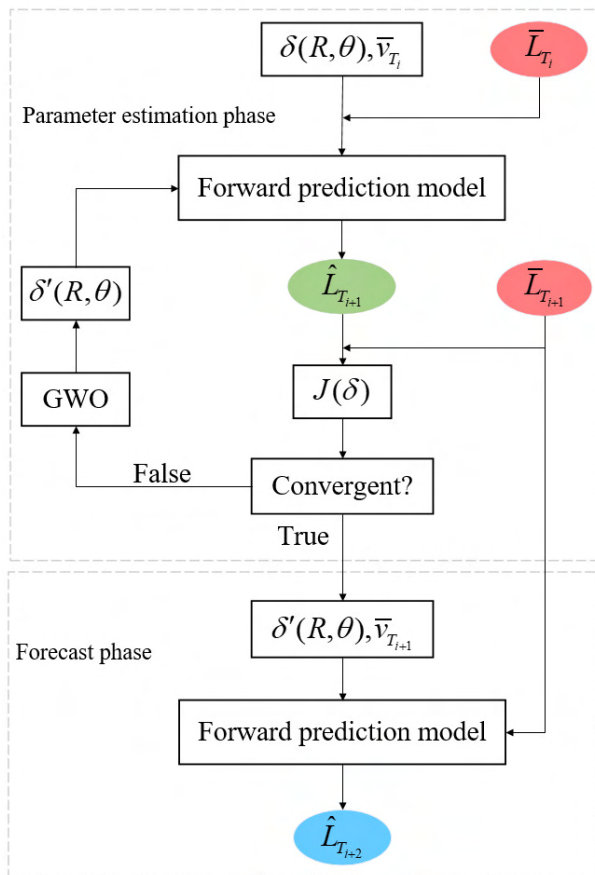


Figure 4: Flow chart of FFPS program structure. The gray dashed box above shows the parameter estimation phase, and the one below is the forecast phase.

#### 3.2 The Forward Prediction Model Based on the Huygens Principle

Fire behavior trend prediction requires a combination of fire parameters and spread theory for boundary expansion (Li et al., 2022). The Huygens principle used to explain light propagation was first applied to fire boundary expansion by Richards (Richards, 1990). The interpretation of the Huygens principle applied to fire spread is shown in Fig. 5, each of the  $N$  discrete points  $P_i^T(x_i^T, y_i^T)$  on the fireline at time  $T$  is taken as an initial point, which expands into a small ellipse after time  $dt$ . The fireline at time  $T + 1$  is the outer envelope of these small ellipses, and  $P_i^{T+1}(x_i^{T+1}, y_i^{T+1})$  is the tangent point between the small ellipse and the outer envelope.

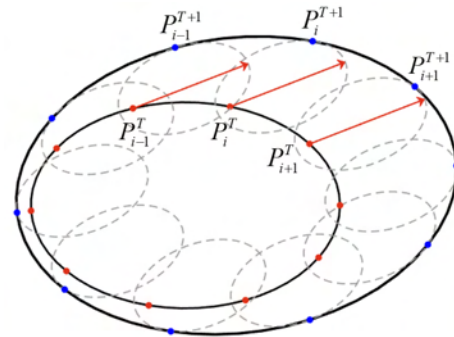


Figure 5: Schematic diagram of the Huygens principle. The red-marked points are the discrete points of the fireline at time  $T$ . The blue points form the predicted fireline at time  $T + 1$ , which are the tangent points of the small ellipses to the forecast fireline. The red arrow represents the main spreading direction  $\theta$ , and the subscript  $i$  is the node flag on the current fireline.

The details of the small ellipse are shown in Fig. 6,  $a$  and  $(b + c)$  are the flanking spreading rate and the forward spreading rate of the small ellipse (Richards, 1993). The arrow represent the main spreading direction  $\theta$  at  $P_i^T$  and the spreading distance after time  $dt$ .

The coordinate of the point  $P_i^{T+1}$  on the outer envelope curve is calculated by the Eq. (3) and Eq. (4):

$$x_i^{T+1} = \left( \frac{a^2 S_1 \cos \theta - b^2 S_2 \sin \theta}{\sqrt{b^2 (S_2)^2 + a^2 (S_1)^2}} + c \sin \theta \right) \times dt + x_i^T \quad (3)$$

$$y_i^{T+1} = \left( \frac{-a^2 S_1 \sin \theta - b^2 S_2 \cos \theta}{\sqrt{b^2 (S_2)^2 + a^2 (S_1)^2}} + c \cos \theta \right) \times dt + y_i^T \quad (4)$$

where

$$S_1 = x_s \sin \theta + y_s \cos \theta \quad (5)$$

$$S_2 = x_s \cos \theta - y_s \sin \theta \quad (6)$$

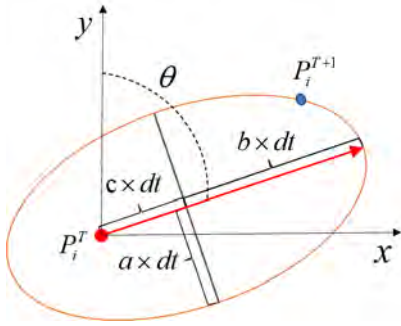


Figure 6: Schematic diagram of the small ellipse expansion.

$$x_s = \frac{(x_{i+1}^T - x_{i-1}^T) \times N}{4\pi} \quad (7)$$

$$y_s = \frac{(y_{i+1}^T - y_{i-1}^T) \times N}{4\pi} \quad (8)$$

$a, b, c$  can be calculated by the geometric relationship between the length-to-width ratio  $LB$  of the small ellipse and  $R$ :

$$a = R \frac{1 + 1/HB}{2LB} \quad (9)$$

$$b = R \frac{1 + 1/HB}{2} \quad (10)$$

$$c = b - \frac{R}{LB} \quad (11)$$

$LB$  and  $HB$  are calculated by the wind speed  $U$  (m/s) in the middle of the flame:

$$LB = 0.936e^{0.2566U} + 0.461e^{-0.1548U} - 0.397 \quad (12)$$

$$HB = (LB + \sqrt{LB^2 - 1}) / (LB - \sqrt{LB^2 - 1}) \quad (13)$$

The wind speed in the middle of the flame is considered to be equivalent to the wind speed of the sensor, i.e.  $U = v$ . The main spreading direction  $\theta$  is the resultant vector of wind direction and slope direction, which is calculated according to the method in Farsite, and it is both the input to the traditional model and the initial value for parameter estimation.

### 3.3 Cost Function

An appropriate cost function  $J$  must be defined to minimize the difference to estimate the dynamic parameters  $\delta(R, \theta)$  when both predicted and observed firelines are available.  $J$  is defined as the sum of the Euclidean distances from the predicted fireline to the corresponding observed fireline, and the formula is shown

in Eq. (14).

$$J(\delta, T) = \sum_{i=1}^N |\bar{P}^i - \hat{P}^i| = |\bar{L} - \hat{L}| = |\bar{L} - F(\delta, \bar{v})| \quad (14)$$

$\hat{P}^i$  is the point on the predicted fireline  $\hat{L}$  at time  $T$ , where the normal intersects the real fireline  $\bar{L}$  with  $\bar{P}^i$ , and  $F(\delta, \bar{v})$  is the fireline prediction function.

Once the cost function has been defined, the problem of solving for the optimal dynamic variable  $\delta(R, \theta)$  is equivalent to the problem of minimizing  $J$ :

$$\min J(\delta) \begin{cases} R \in [0, 5](m/\min) \\ \theta \in [0, 2\pi](rad) \end{cases} \quad (15)$$

The definition domain of  $R$  is derived from empirical values.

### 3.4 Optimization Algorithm

Eq. (15) is a constrained optimization problem, and a suitable optimization method needs to be found to solve it. The numerical optimization method is usually applied to solve the nonlinear inverse problem (Meng, 2019), and it can be divided into the deterministic method and the non-deterministic search method (Amoialis et al., 2014). The former is mainly based on gradient calculation, which is faster to converge, but easily falls into local optimum. The latter is gradient-free and the global optimum can be found, but it is computationally intensive when with too many variables. This system is a highly linearized system and has few solution variables, therefore non-deterministic search method are more suitable.

Mirjalili proposed the Grey Wolf Optimizer (GWO) by simulating the pack hunting behavior of grey (Mirjalili et al., 2014). The GWO is characterized by simple structure, few adjustment parameters, robustness to its own parameter changes, and the convergence factor can be adaptively adjusted during the iteration. In addition, its search individual is equipped with information feedback mechanism, and the relationship between local search and global search can be balanced, so its performance is better in terms of solution accuracy and convergence speed. With the requirements for operation speed and accuracy, the GWO is chosen for minimizing  $J$  in this paper.

## 4 RESULTS AND ANALYSIS

### 4.1 Fire Boundary Prediction

A ROS model must be chosen and then combines with the forward model as a traditional method for comparison with FFPS. Among the commonly used ROS models, the Rothermel formula based on the law of energy conservation requires more parameters that are not easily

accessible, and the McArthur model is only applicable to a few specific fuel types. Wang Zhengfei proposed a ROS model with simple parameters and a wide range of adaptations for the forest scenario in China, so Wang Zhengfei model is chosen as the traditional model for comparison in this paper. The modified Wang's formula (Zhang et al., 2020) is presented in Eq. (16):

$$R = 1.0372 \times K_s \times e^{0.1783 \times v + 3.533 \times (\tan \varphi)^{1.2} - 0.057 \times m} \quad (16)$$

where  $m$  is the fuel moisture content,  $K_s$  is the fuel correction factor that can be obtained by consulting the graph in the literature (Wang, 1983),  $v(m/s)$  is the wind speed, and  $\varphi$  ( $^\circ$ ) is the slope.

This system and the traditional method were predicted separately using the experimental data in Section 2, and the results are shown in Fig. 7. Where red is the observed fireline, green and blue represent the predicted fireline for the conventional method and FFPS. The prediction of the traditional shows a large difference from the real fireline, while the FFPS-GWO has only a small difference.

## 4.2 Parameter Estimation

The comparison of the ROS calculated by Eq. (16) and after parameter estimation is shown in Fig. 8(a), and there are huge gaps between them. The trends are similar but exponentially different in value, with the maximum and the minimum difference of  $1.73m/min$  and  $0.78m/min$ .

The comparison of main spreading direction is shown in Fig. 8(b), the trends of change are similar, but the differences reached  $44^\circ$  and  $36^\circ$  at  $T = 30s$  and  $40s$ .

## 4.3 Error Analysis

In addition to comparing with traditional model, the classical intelligent swarm algorithms Genetic Algorithm (GA) (Whitley, 1994) and Particle Swarm Optimization (PSO) (Wang et al., 2018) were added to FFPS for accuracy comparison, and two evaluation criteria are chosen for both fire area and fire perimeter respectively: Confusion Matrix (Yang et al., 2019) and Hausdorff distance (Rote, 1991).

### 4.3.1 Confusion Matrix

Except for the correctly predicted part, the over-predicted and unpredicted parts are also present in the prediction results. This error can be described by constructing confusion Matrix to calculate Commission Error ( $CE$ ) and Omission Error ( $OE$ ). As shown in Fig. 9,  $(MP + CP)$  and  $(EP + CP)$  means the real fire area and the predicted fire area respectively.  $CE$  is the proportion of the error area in the total predicted fire area;  $OE$  is the proportion of the omitted area in

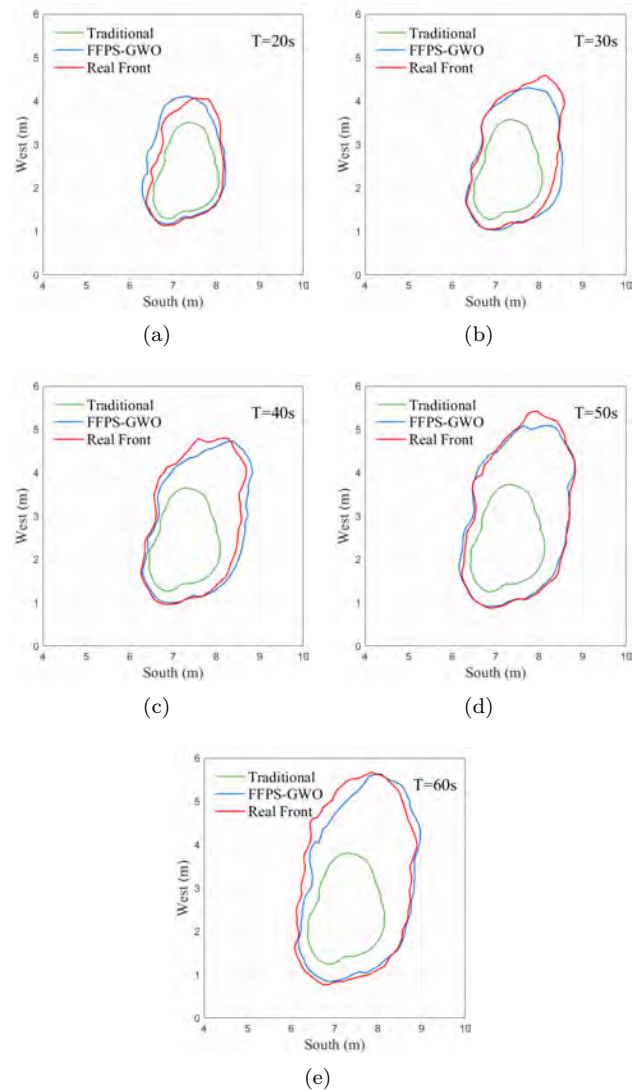


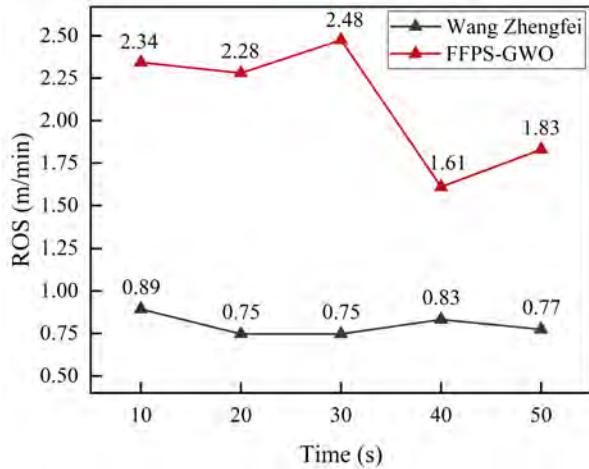
Figure 7: Comparison of predicted (traditional model and FFPS-GWO) and observed firelines at different times.

the real fire area. Better predictions are evidenced by smaller  $CE$  and  $OE$ .

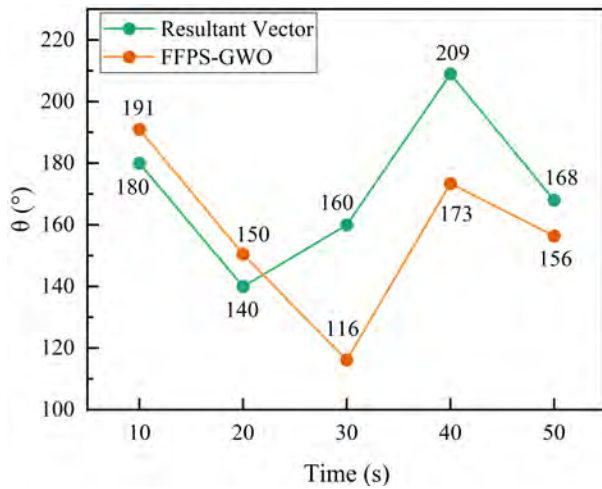
The  $CE$  and  $OE$  are calculated by Eq. (17):

$$\begin{cases} CE = 1 - \frac{CP}{EP+CP} \\ OE = 1 - \frac{CP}{CP+MP} \end{cases} \quad (17)$$

As shown in Fig. 10, The  $CE$  of the traditional method is 0 at all times, but the minimum value of  $OE$  is 39%. The explanation for this phenomenon can be obtained in Fig. 7 and Fig. 8. The traditional model has a small value of ROS so its predicted region is a subset of the real region, thus there is no over-predicted area but a



(a)



(b)

Figure 8: (a) The comparison of ROS calculated by Wang Zhengfei model and optimized by FFPS-GWO. (b) Comparison of main spreading direction  $\theta$ , resultant vector is the initial main direction calculated by the formula.

large proportion of unpredicted area. The CE of FFPS-GA is 1% while the OE is 18% when  $T = 30s$ , thus it has more unpredicted area.

And the average CE of FFPS-PSO and FFPS-GWO are 6.35%, 5.8%, and the average OE are 6.99%, 6.94%, so FFPS-GWO performs better in confusion matrix.

### 4.3.2 Hausdorff Distance

The similarity between the sets of discrete points can be measured by the Hausdorff distance, so that the difference between the predicted and the real fire perimeters can be evaluated. The Hausdorff distance is defined as the maximum of all distances from the nearest

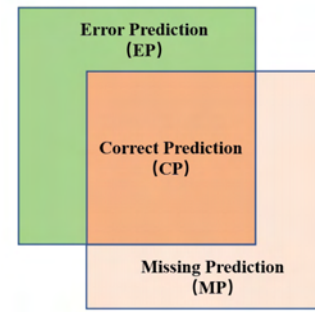
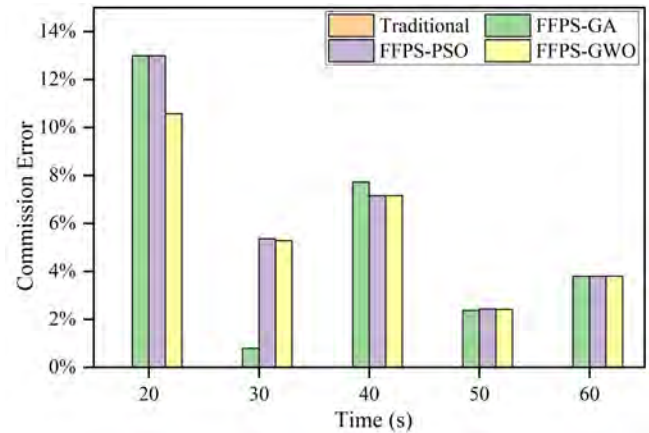
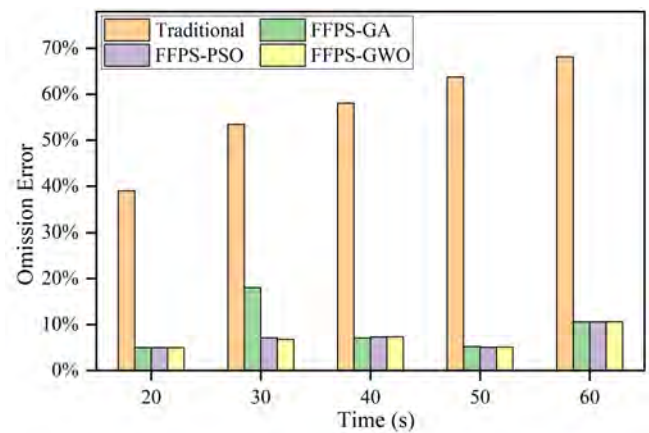


Figure 9: The schematic of commission error and omission error.  $(EP + CP)$  is the fire area predicted by the model, and  $(MP + CP)$  is the real fire area.



(a)



(b)

Figure 10: (a) Comparison of commission errors of four model simulations. (b) Comparison of omission errors of four model simulations.

point in a set to another set. The observed and predicted point sets of the fireline are  $U = \{u_1, \dots, u_n\}$  and

$V = \{v_1, \dots, v_n\}$ , then the Hausdorff distance between them is defined as:

$$H(U, V) = \max(h(U, V), h(V, U)) \quad (18)$$

where

$$h(U, V) = \max_{u \in U} \min_{v \in V} \|u - v\| \quad (19)$$

$$h(V, U) = \max_{v \in V} \min_{u \in U} \|v - u\| \quad (20)$$

$\|\bullet\|$  is the normative distance between point sets  $U$  and  $V$ . The smaller the Hausdorff distance, the closer the two point sets are, which means better predictions.

The calculated Hausdorff distance is shown in Fig. 11, and the traditional method reached a maximum value of  $1.95m$  at  $T=60s$ , which is considerably greater than the FFPS. The results of FFPS equipped with GA, PSO, and GWO are similar, with average values of  $0.334m$ ,  $0.340m$ , and  $0.324m$ .

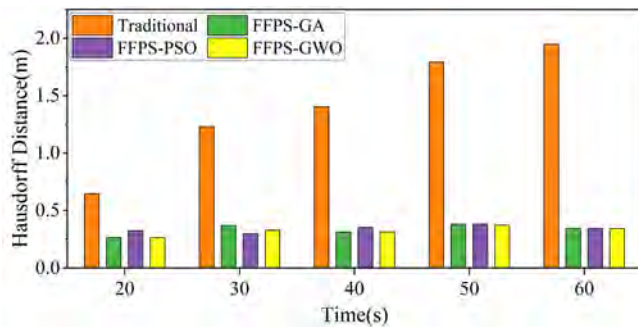


Figure 11: Comparison of Hausdorff distance between simulated and actual results of the four models.

#### 4.4 The Comparison of Algorithm Performance

The obvious accuracy difference is not reflected in the FFPS with the three different algorithms in the Section 4.3, therefore, their number of iterations and operation time were compared.

In Fig. 12, the minimum number of iterations for GA and PSO are 72 and 44, which are both larger than that of GWO. The reason for all iterations of GWO being 15 is that the maximum number of iterations was set manually. And after several tests, 15 was verified to be the minimum number of iterations that could achieve the optimal result.

The Tab. 1 shows that the average running time of GWO is much smaller than that of GA and PSO. Compared with other two algorithms, the total number of iterations of GWO is reduced by 86.1% and 74.3%, and the average running time is reduced by 88.8% and 91.4%.

In summary, the computational cost of GWO is extremely low in the case of smaller errors, and thus it is more suitable to be applied to FFPS.

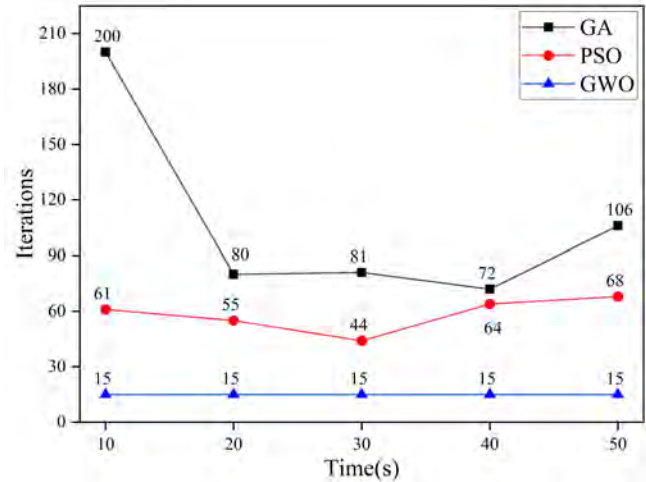


Figure 12: Comparison of the iterations of GA, PSO, and GWO algorithms at each time node.

Table 1: Average running time of GA, PSO, and GWO.

Algorithm	GA	PSO	GWO
Average running time(s)	9.2323	12.1215	1.037

#### 4.5 Discussion

From the above results, it is shown that FFPS improves the prediction accuracy of the fireline compared to the traditional method. In addition, GWO performs well compared to the other two optimization algorithms and improves the operation speed and prediction accuracy of the system, and the following is an analysis of the results and problems. The reasons for the differences between the optimized and calculated values for the two dynamic variables are analyzed as follows. For the ROS, first of all, the data used to derive Wang Zhengfei's formula came from indoor combustion experiments in southwestern China, while the experimental site in this paper is outdoors in northeastern China, where the climatic environment and the nature of combustible materials differ greatly. Secondly, the fire boundary prediction using the ROS calculated by the traditional formula in the direction of the fire head may not be suitable, while the optimized ROS is more biased towards the global velocity of the fire, which may include the correction of the errors in the prediction model, sensors, etc. For the main spread direction  $\theta$ , there are inevitable computational errors in the synthesis of vectors with different magnitudes, in addition, the internal weather of the fire is affected by the combustion, and the optimized  $\theta$  solves these problems.

For shape prediction error, compared with the traditional forest fire spread model, the average OE of FFPS-

GWO was reduced by 87.7% and the average Hausdorff distance was reduced by 76.9%. Although FFPS-GWO achieves a relatively good prediction accuracy, there are still some errors, which are analyzed as follows. First, the influence of the local location of the experimental site equipped with non-homogeneous combustibles on the fire was not adequately taken into account by the prediction model. Second, the accuracy of the extracted real fireline can be affected by the errors of the IR camera and the marker points. Then, the actual tendency of the fire spread will be influenced by the coupling effect of the fire and the atmosphere, which is not considered by the model. Furthermore, the accuracy of parameters estimation are affected by the way in which the cost function is defined.

For the optimization, it is worth pointing out that the number of iterations of the GWO is set manually, and the results that outperform the other two algorithms at lower iterations are still derived by GWO, thus significantly reducing the running time. It indicates that the algorithm has strong robustness and is able to achieve a balance between local and global optimization by adaptively adjusting the convergence factor and information feedback mechanism.

## 5 CONCLUSION

In this paper, the parameter estimation and data-driven forest fire spread prediction system is proposed, and the two dynamic variables that have the greatest influence on fire behavior prediction, the rate of fire spread and the main spread direction, are estimated by it through minimizing the difference between observed and predicted firelines, and the accurate real-time predictions are achieved by combining corrected parameters and multi-sensor data. The burn experiment was designed and performed, and the real fire data came from infrared camera carried by the UAV and wind sensors on the ground. With the validation of real data, The average commission and omission error of this system are 5.8% and 6.94%, and the average Hausdorff distance is 0.324m, which greatly improves the prediction accuracy compared with traditional method. In addition, compared with PSO and GA, the average computation time of the GWO in this system is only 1.037s, which has a great computational efficiency. In summary, the FFPS-GWO can quickly and accurately obtain predicted firelines, which is of great importance for the correct deployment of firefighting forces and provides a theoretical basis for predicting large-scale fire in real scenarios. In future work, the method proposed in this paper will be applied to different scenarios and continuously improved based on the results, thus enhancing its applicability.

## ACKNOWLEDGEMENT

This work was supported by Natural Science Foundation of Heilongjiang Province of China (Grant No.LH2020C042); China University Industry-Education-Research(IER) Innovation Fund(Grant No. 2021ZYA12006). Thanks are also due to the MCFNS anonymous reviewers.

## REFERENCES

- Alessandri, A., Bagnerini, P., Gaggero, M., and Mantelli, L. (2021). Parameter estimation of fire propagation models using level set methods. *Applied Mathematical Modelling*, 92:731–747.
- Altintas, I., Block, J., De Callafon, R., Crawl, D., Cowart, C., Gupta, A., Nguyen, M., Braun, H.-W., Schulze, J., Gollner, M., et al. (2015). Towards an integrated cyberinfrastructure for scalable data-driven monitoring, dynamic prediction and resilience of wildfires. *Procedia Computer Science*, 51:1633–1642.
- Amoiralis, E. I., Tsili, M. A., Paparigas, D. G., and Kladas, A. G. (2014). Global transformer design optimization using deterministic and nondeterministic algorithms. *IEEE Transactions on Industry Applications*, 50(1):383–394.
- Anderson, K., Reuter, G., and Flannigan, M. D. (2007). Fire-growth modelling using meteorological data with random and systematic perturbations. *International Journal of Wildland Fire*, 16(2):174–182.
- Cardil, A., Monedero, S., Schag, G., de Miguel, S., Tapia, M., Stooft, C. R., Silva, C. A., Mohan, M., Cardil, A., and Ramirez, J. (2021). Fire behavior modeling for operational decision-making. *Current Opinion in Environmental Science & Health*, 23:100291.
- Carrasco, J., Pais, C., Shen, Z.-J. M., and Weintraub, A. (2019). Adjusting rate of spread factors through derivative-free optimization: a new methodology to improve the performance of forest fire simulators. *arXiv preprint arXiv:1909.05949*.
- Choi, B.-D., Han, J.-W., Kim, C.-S., and Ko, S.-J. (2006). Frame rate up-conversion using perspective transform. *IEEE Transactions on Consumer Electronics*, 52(3):975–982.
- Denham, M., Wendt, K., Bianchini, G., Cortés, A., and Margalef, T. (2012). Dynamic data-driven genetic algorithm for forest fire spread prediction. *Journal of Computational Science*, 3(5):398–404.

- Erkan, U., Gökrem, L., and Enginoğlu, S. (2018). Different applied median filter in salt and pepper noise. *Computers & Electrical Engineering*, 70:789–798.
- Ferragut, L., Asensio, M., Cascón, J., and Prieto, D. (2015). A wildland fire physical model well suited to data assimilation. *Pure and Applied Geophysics*, 172(1):121–139.
- Finney, M. A. (1998). Farsite: Fire area simulator-model development and evaluation. *USDA Forest Service - Research Papers RMRS*, (RP-4).
- Griffiths, D. (1999). Improved formula for the drought factor in mcarthur’s forest fire danger meter. *Australian Forestry*, 62(2):202–206.
- Lagarias, J. C., Reeds, J. A., Wright, M. H., and Wright, P. E. (1998). Convergence properties of the nelder-mead simplex method in low dimensions. *SIAM Journal on optimization*, 9(1):112–147.
- Li, X., Zhang, M., Zhang, S., Liu, J., Sun, S., Hu, T., and Sun, L. (2022). Simulating forest fire spread with cellular automation driven by a lstm based speed model. *Fire*, 5(1):13.
- Mandel, J., Beezley, J. D., Coen, J. L., and Kim, M. (2009). Data assimilation for wildland fires. *IEEE Control Systems Magazine*, 29(3):47–65.
- Meng, Z. (2019). Survey on inverse problem and its inversion methods of impact dynamics. *Science Technology and Engineering*, 19(04):1–8.
- Mirjalili, S., Mirjalili, S. M., and Lewis, A. (2014). Grey wolf optimizer. *Advances in engineering software*, 69:46–61.
- Monedero, S., Ramirez, J., and Cardil, A. (2019). Predicting fire spread and behaviour on the fireline. wild-fire analyst pocket: A mobile app for wildland fire prediction. *Ecological Modelling*, 392:103–107.
- Norouzi, A., Rahim, M. S. M., Altameem, A., Saba, T., Rad, A. E., Rehman, A., and Uddin, M. (2014). Medical image segmentation methods, algorithms, and applications. *IETE Technical Review*, 31(3):199–213.
- Richards, G. D. (1990). An elliptical growth model of forest fire fronts and its numerical solution. *International journal for numerical methods in engineering*, 30(6):1163–1179.
- Richards, G. D. (1993). The properties of elliptical wild-fire growth for time dependent fuel and meteorological conditions. *Combustion science and technology*, 95(1-6):357–383.
- Rochoux, M. C., Delmotte, B., Cuenot, B., Ricci, S., and Trouvé, A. (2013). Regional-scale simulations of wildland fire spread informed by real-time flame front observations. *Proceedings of the Combustion Institute*, 34(2):2641–2647.
- Rote, G. (1991). Computing the minimum hausdorff distance between two point sets on a line under translation. *Information Processing Letters*, 38(3):123–127.
- Rothermel, R. (1972). A mathematical model for predicting fire spread in wildland fuels. *Usda Forest Service General Technical Report*, 115.
- Srivas, T., de Callafon, R. A., Crawl, D., and Altintas, I. (2017). Data assimilation of wildfires with fuel adjustment factors in farsite using ensemble kalman filtering. *Procedia Computer Science*, 108:1572–1581.
- Tolhurst, K., Shields, B., and Chong, D. (2008). Phoenix: development and application of a bushfire risk management tool. *Australian journal of emergency management*, 23(4):47–54.
- Tymstra, C., Bryce, R., Wotton, B., Taylor, S., Armitage, O., et al. (2010). Development and structure of prometheus: the canadian wildland fire growth simulation model. *Natural Resources Canada, Canadian Forest Service, Northern Forestry Centre, Information Report NOR-X-417*.(Edmonton, AB).
- Wang, D., Tan, D., and Liu, L. (2018). Particle swarm optimization algorithm: an overview. *Soft computing*, 22:387–408.
- Wang, Z. (1983). The measurement method of the wildfire initial spread rate. *Mountain Research*, 1(2):42–51.
- Whitley, D. (1994). A genetic algorithm tutorial. *Statistics and computing*, 4(2):65–85.
- Yang, N., Qian, Y., EL-Mesery, H. S., Zhang, R., Wang, A., and Tang, J. (2019). Rapid detection of rice disease using microscopy image identification based on the synergistic judgment of texture and shape features and decision tree-confusion matrix method. *Journal of the Science of Food and Agriculture*, 99(14):6589–6600.
- Yu, J., Gao, N., Meng, Z., and Zhang, Z. (2021). High-accuracy projector calibration method for fringe projection profilometry considering perspective transformation. *Optics Express*, 29(10):15053–15066.
- Zhang, X., Liu, P., and Wang, X. (2020). Research on improvement of wang zhengfei’s forest fire spread model. *Journal of Shandong Forestry Science and Technology*, 50(01):1–6.